Molecular Dynamics Simulations of the Anticodon Hairpin of $tRNA^{Asp}$: Structuring Effects of C−H···O Hydrogen Bonds and of Long-Range Hydration Forces

Pascal Auffinger, Shirley Louise-May, and Eric Westhof*

Contribution from the Institut de Biologie Moléculaire et Cellulaire du CNRS, Modélisations et Simulations des Acides Nucléiques, UPR 9002, 15 rue René Descartes, 67084 Strasbourg Cedex, France

Received July 25, 1995[⊗]

Abstract: The inclusion of long-range *solvent* interactions out to 16 Å in a molecular dynamics study of the anticodon loop of $tRNA^{Asp}$ led to an overall structural stabilization of the RNA hairpin tertiary interactions in a set of six independent fully solvated and neutralized 100 ps MD trajectories as compared to a shorter-ranged *solvent* interaction electrostatic model (8 Å). The increased structural stabilization allowed for the emergence of non-classical C−H···O hydrogen bonds in the MD trajectories. The presence of the C−H···O hydrogen bonds in the crystal structure was subsequently verified and dynamically characterized and their contribution to the preservation of the tertiary native conformation was assessed. The MD trajectories generated using a truncation distance of 16 Å for the electrostatic *solute*−*solvent* and *solvent*−*solvent* interactions, with no cutoffs applied to the electrostatic *solute*−*solute* interactions, compared to an earlier set of eight independent 100 ps MD trajectories using a smaller truncation distance of 8 Å (Auffinger, P.; Louise-May, S.; Westhof, E. *J. Am. Chem. Soc.* **1995**, *117,* 6720−6726), revealed an increase in consistency of structural characteristics between individual MD trajectories of a given set and on average a decrease in root-mean-square deviation values from the starting crystal structure. Dihedral transitions in the sugar−phosphate backbone decreased and tertiary interactions specific to the loop topology were better preserved and showed reduced dynamical fluctuation. These results emphasize the important influence of long-ranged solvation forces on the stabilization of the tertiary structure of highly charged nucleic acid systems and signify that long-ranged theoretical models may be necessary for a truly accurate description of biomacromolecular solution structure and dynamics.

Introduction

In aqueous systems of biological macromolecules, short-ranged *solute*−*solute* interactions, through covalent bonds, hydrogen bonds, or short van der Waals interactions, are believed to play a central role in tertiary structure determination.[1,2] Direct *solute*−*solvent* interactions, which have been visualized crystallographically, are also found to actively contribute to tertiary structural stabilization, especially for nucleic acids.[3−5] However, the effects of long-range *solute*−*solvent* and *solvent*−*solvent* forces, relatively small on a per interaction basis and not yet well understood,[6,7] comprise the vast majority of the number of potential interactions present in the system and may have a large structurally determining effect. In the application of molecular dynamics to systems of biological interest, resource limitations have only incrementally allowed for inclusion of these hydration forces. As more accurate theoretical models became accessible, the inclusion of longer-ranged forces consistently and demonstrably improved stability and correlation between experimental and calculated structural and dynamical properties.[8−13]

The current trend toward extending the MD time scale to the nanosecond regime using relatively short truncation distances in the calculation of electrostatic interactions (8−10 Å) does not reflect an appreciation for longer range effects of hydration forces which have been reported to alter not only the solvent dynamics of the system but also the solute structural conformation and overall system stabilization as well.[8,14−16] Although many papers which have addressed the issue of extending truncation distances found modifications of the dynamic structures of the solute as well as of the solvent, both in the bulk and in the vicinity of the solute,[10,14−17] these effects were mostly attributed to the greater accuracy with which the *solute*−*solute* interactions were calculated. However, Madura and Pettitt[18] noted that, in a periodic system consisting of a Cl^- ion in a box of water molecules, increasing the truncation distances

* Author to whom correspondence should be addressed: phone (33) 88-41-70-46; FAX (33) 88-60-22-18; E-mail westhof@astorg.u-strasbg.fr.

[⊗] Abstract published in *Advance ACS Abstracts,* December 15, 1995.

(1) Saenger, W. *Principles of Nucleic Acid Structure*; Springer-Verlag: New York, 1984.
(2) Jeffrey, G. A.; Saenger, W. *Hydrogen Bonding in Biological Structures*; Springer-Verlag: Berlin, 1991.
(3) Westhof, E. *Annu. Rev. Biophys., Biophys. Chem.* **1988**, *17*, 125−144.
(4) Westhof, E.; Beveridge, D. L. *Hydration of Nucleic Acids*; Westhof, E., Beveridge, D. L., Eds.; Cambridge University Press: Cambridge, 1990; pp 24−123.
(5) Westhof, E. *Structural Water of Nucleic Acids*; Westhof, E., Ed.; 1990; pp 11−18.
(6) Israelachvili, J. *Acc. Chem. Res.* **1987**, *20*, 415−421.
(7) Leikin, S.; Parsegian, V. A.; Rau, D. C. *Annu. Rev. Phys. Chem.* **1993**, *44*, 369−395.
(8) Smith, P. E.; Pettitt, B. M. *J. Chem. Phys.* **1991**, *95*, 8430−8441.
(9) Kitson, D. H.; Avbelj, F.; Moult, J.; Nguyen, D. T.; Mertz, J. E.; Hadzi, D.; Hagler, A. T. *Proc. Natl. Acad. Sci. U.S.A.* **1993**, *90*, 8920−8924.
(10) York, D. M.; Darden, T.; Pedersen, L. G. *J. Chem. Phys.* **1993**, *99*, 8345−8348.
(11) York, D. M.; Wlodawer, A.; Pedersen, L. G.; Darden, T. A. *Proc. Natl. Acad. Sci. U.S.A.* **1994**, *91*, 8715−8718.
(12) York, D. M.; Yang, W.; Lee, H.; Darden, T.; Pedersen, L. G. *J. Am. Chem. Soc.* **1995**, *117*, 5001−5002.
(13) Cheatham, T. E.; Miller, J. L.; Fox, T.; Darden, T. A.; Kollman, P. A. *J. Am. Chem. Soc.* **1995**, *117*, 4193−4194.
(14) Schreiber, H.; Steinhauser, O. *Biochemistry* **1992**, *31*, 5856−5860.
(15) Schreiber, H.; Steinhauser, O. *J. Mol. Biol.* **1992**, *228*, 909−923.
(16) Schreiber, H.; Steinhauser, O. *Chem. Phys.* **1992**, *168*, 75−89.
(17) Steinbach, P. J.; Brooks, B. R. *J. Comput. Chem.* **1994**, *15*, 667−683.
(18) Madura, J. D.; Pettitt, B. M. *Chem. Phys. Lett.* **1988**, *150*, 105−108.

0002-7863/96/1518-1181$12.00/0

altered the shape of the ion−water radial distribution functions. Straatsma and Berendsen[19] showed that modifying only the *solvent−solvent* truncation distances changed the calculated hydration free energy of an Ne atom to an Na^+ ion perturbation calculation in water. Alper et al.[20,21] studied the influence of long-range forces on the water structure above a phospholipid monolayer−water system. Selectively varying the *lipid−water* and the *water−water* truncation distances, they deduced that the protocol changes significantly affected the water dynamics. In the present study we report the results of inclusion of long-ranged hydration forces on the system stability as well as on the solute conformation and dynamics.

Increased stabilization due to a more accurate theoretical description of the system may reveal other stabilizing tertiary interactions not prominent in the data analyses of traditional structural determination experiments. To date, no C−H···O hydrogen bonds have been described in the known crystal structures of RNA molecules, due in part to the insufficient resolution of the crystallographic diffraction patterns. Additionally, C−H···O hydrogen bonds were not previously considered as contributing significantly to the stability of biomolecules. However, a growing body of evidence, coming mostly from neutron diffraction data on small molecules, show that C−H···O bonds may have a significant influence in the structural chemistry of a great range of systems.[2,22,23] Taylor and Kennard[24] showed that C−H···O contacts are electrostatic by nature and that they occur for C···O distances between 3.0 and 4.0 Å with C−H···O angles between 90° and 180°. Desiraju[22] stated that the energy of such C−H···O bonds (1−2 kcal/mol) falls in a range where they can either compete or contribute with other conformational forces. The strength of these bonds is variable and depends on the acidity of the C−H groups. Nucleic acids make good candidates for such C−H bonds with other constituents because proximal intraresidue protonated nitrogens act to modifiy the acidity of the C−H group making it a more suitable hydrogen bond donor.[1,3] Jeffrey and Saengers[2] report that in many nucleoside and nucleotide crystal structures, the C6···O5′ or C8···O5′ distances are in the 3.0 to 3.2 Å range suggesting H···O5′ hydrogen bonds between 2.0 and 2.2 Å. These distances correspond to the shorter of those reported for C−H···O interactions. C−H···O hydrogen bonds have also been suggested to participate in the stabilization of nucleotides,[1,25] of standard base pairs as well as mismatches.[26] An analysis of possible C−H···O hydrogen bonds present in the crystal structure of the tRNA hairpin, the frequency of occurrence, and the dynamical character of these bonds as determined from the MD trajectories was therefore conducted in the present study.

It may be argued that extension of the MD time scale is necessary to demonstrate system stabilization; i.e., How long does it take to effect structural equilibrium for the system and how far does this equilibrium reside from the starting configuration? Recently, an upper bound of 100 ns has been proposed on the basis of theoretical and experimental work.[27,28] Unfortunately, such time scales are beyond our existing computational means. Furthermore, the accumulation of statistical errors over longer trajectories is not trivial and should be considered by including systematic testing for each new protocol used in order to determine its range of applicability. Another way to sample the theoretical configurational space of a given system, and to detect protocol instabilities, can come from running multiple molecular dynamics trajectories on a shorter time scale, generating unique trajectories which, as an ensemble, have the advantage of more accurately describing the modeled system properties and dynamics closer to the region of the starting configuration. In our previous work utilizing an 8 Å truncation distance for *solute−solvent* and *solvent−solvent* interactions, the multiple molecular dynamics approach revealed that the chosen protocol did not lead to enough consistency between independent MD trajectories to warrant meaningful structural analyses of the results.[29] We concluded that it would be highly unlikely for any of the generated trajectories to exhibit an extended structural equilibrium in the vicinity of the starting structure upon extension of the trajectory to the nanosecond regime and thus that other protocols should be investigated. In the improved protocol set of MD trajectories discussed here, the multiple MD trajectory approach was again utilized to afford an estimate of protocol, system, and structural stability.

As in our preceding work, we calculated explicitely all *solute−solute* interactions applying no truncation distance to them; it was thus inferred that other interactions must play a role in the structural stabilization of the anticodon loop. Our aim in this investigation was to assess the effect of long-range hydration forces on system and structural stabilization as well as solute dynamics. Therefore, we have made a comparison of two sets of MD trajectories in which the long-ranged *solvent* interactions have been more accurately accounted for in one set by extending the truncation distances for interactions involving the solvent from 8 to 16 Å. Global and per-residue root-mean-square (rms) deviations addressing the relative extent of system stabilization are presented. Analysis of the frequency of dihedral transitions and the time-averaged values and dynamical behavior of intramolecular hydrogen bonds conveys the amount of structural stabilization exhibited in each of the two sets. Finally, the contribution of nonclassical and C−H···O hydrogen bonds to the stabilization of the tertiary native conformation is explored and discussed.

Computational Procedure

The protocol and the starting coordinates used to generate the six 100-ps MD trajectories of the 17 bases of the anticodon hairpin of $tRNA^{Asp}$ (Figure 1) neutralized by 16 NH_4^+ counterions discussed here correspond to those used in our preceding paper.[29] The main differences lie in the treatment of the long-range electrostatic interactions. *Solute−solvent* and *solvent−solvent* interaction truncation distances were increased from 8 to 16 Å. In Figure 2, we illustrate this difference at a local level by showing at the left all water molecules located at 8 Å around the phosphorus atom of residue G30 and at the right all water molecules located at 16 Å around the same point. For the entire system, the increase in truncation distance caused the number of SPC/E water molecules[30] solvating the solute to increase from 2856 to 3765 and the size of the solvation box likewise increased from 55.7 × 43.2 × 42.7 to 59.7 × 47.2 × 46.7 $Å^3$, accommodating consequently more than

(19) Straatsma, T. P.; Berendsen, H. J. C. *J. Chem. Phys.* **1988**, *89*, 5876−5886.
(20) Alper, H. E.; Bassolino, D.; Stouch, T. R. *J. Chem. Phys.* **1993**, *98*, 9798−9818.
(21) Alper, H. E.; Bassolono-Klimas, D.; Stouch, T. R. *J. Chem. Phys.* **1993**, *99*, 5547−5559.
(22) Desiraju, G. R. *Acc. Chem. Res.* **1991**, *24*, 290−296.
(23) Steiner, T.; Saenger, W. *J. Am. Chem. Soc.* **1992**, *114*, 10146−10154.
(24) Taylor, R.; Kennard, O. *J. Am. Chem. Soc.* **1982**, *104*, 5063−5070.
(25) Rao, S. T.; Sundaralingam, M. *J. Am. Chem. Soc.* **1970**, *92*, 4963−4970.
(26) Leonard, G. A.; McAuley-Hecht, K.; Brown, T.; Hunter, W. N. *Acta Crystallogr.* **1995**, *D51*, 136−139.
(27) Caspar, D. L. D. *Structure* **1995**, *3*, 327−329.
(28) Clarage, J. B.; Romo, T.; Andrews, B. K.; Pettitt, B. M.; Phillips, G. N. *Proc. Natl. Acad. Sci. U.S.A.* **1995**, *92*, 3288−3292.
(29) Auffinger, P.; Louise-May, S.; Westhof, E. *J. Am. Chem. Soc.* **1995**, *117*, 6720−6726.
(30) Berendsen, H. J. C.; Grigera, J. R.; Straatsma, T. P. *J. Phys. Chem.* **1987**, *97*, 6269−6271.

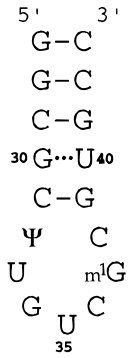

Figure 1. Two-dimensional representation of the anticodon loop of $tRNA^{Asp}$. Ψ and m^1G notations refer to the nonstandard pseudouridine and 1-methylguanine residues.

five solvation shells around the RNA fragment. The *solute−solute* interactions were calculated as before,[29] without truncation distances, thus all RNA−RNA, RNA−NH_4^+, and NH_4^+−NH_4^+ interactions were taken into account explicitely at each step. Such a procedure has been chosen since truncation distances applied to the evaluation of electrostatic interactions between charged groups have been shown to generate severe artifacts which strongly affect the solute structure.[8−10,13] This remains true even for large 16 Å truncation distances.[31]

In the following analysis, comparison is made of the present set of six trajectories generated with the 12−16 Å twin-range cutoff (called **Set_16**) to a set of eight trajectories (S1 to S8; see ref 29) extracted from our previous publication and generated with an 8 Å *solute−solvent* and *solvent−solvent* truncation distance (called **Set_8)**. The AMBER4.1 package[32] was used to run both series of simulations at a constant temperature of 298 K and a constant pressure of 1 atm. with a time step of 2 fs, while the nonbonded pair list was updated every 10 time steps (20 fs). The starting coordinates for the system were kept the same for each of the six simulations and were extracted from the crystal structure of $tRNA^{Asp}$.[33] For all simulations, the Pearlman and Kim set of charges derived from low temperature X-ray data of isolated nucleotides was used,[34] and the charges of the Ψ32 and m^1G37 were adapted from those of the standard bases. The charges for the NH_4^+ ions were extracted from the work of Singh et al.[35]

In order to reduce the CPU time required for the calculations with the 16 Å truncation distance, we employed a 12−16 Å twin-range residue based cutoff for the *solute−solvent* and *solvent−solvent* interactions, in which the long-range electrostatic forces between 12 and 16 Å were updated every 10 time steps (20 fs).[9,36] In this method, shorter ranged interactions (<12 Å) are calculated at each step of the simulation whereas longer ranged interactions (between 12 and 16 Å) are only calculated at each update of the nonbonded pair list and kept constant until the next update. The justification for application of this time saving method is that long-range interactions change in magnitude and gradient more slowly than do shorter ranged interactions. Avbelj et al.[37] and York et al.[10] have tested this method and found it to be reliable in their simulations on large solvated proteins in the crystalline environment with inclusion of explicit mobile counterions. The gain in CPU time for our system was significant. On a SGI R4400 machine, 1 ps of MD took ca. 4 h using a 12−16 Å twin-range cutoff, while taking almost 8 h with a full 16 Å truncation distance. With an 8 Å cutoff 1 ps of MD took only 1 h of CPU time.

The equilibration protocol was kept consistent with our previous calculations[29] and consisted of 100 steps of steepest descent minimization applied to the solvent molecules with fixed solute, followed by 5 ps of molecular dynamics at 300 K on the water with fixed RNA and NH_4^+ counterions. Next ensued molecular dynamics of mobile counterions and water molecules at temperatures of 100 (1 ps), 200 (1 ps), and 300 K (5 ps) again with fixed RNA atomic positions. In subsequent steps, no position constraints were applied to the system. The temperature was progressively increased to 298 K in steps of 50 K with 1 ps of MD at each step. Finally, at 298 K, 5 ps of dynamics were run in order to allow the system to equilibrate at room temperature. The thermalization and equilibration phase of the MD protocol thus lasted 22 ps (Figure 3) for each of the six simulations and data were collected over the subsequent 100 ps of trajectory. At each temperature increase, the velocities were reassigned randomly according to a Boltzmann distribution. Six different values of the random seed were used at the 50 K (t = 12 ps, Figure 3) restart leading to six uncorrelated trajectories.[29] The SHAKE algorithm[38] was used at all stages of the simulations to constrain each X−H bond of the system. A 10 $kcal \cdot mol^{-1} \cdot Å^2$ harmonic distance constraint was applied to the three hydrogen bonds of the first GC base pair of the helix in order to prevent any fraying of the stem (Figure 1). The MDdraw program[39] was used to visualize the generated trajectories on a Silicon Graphics workstation.

Results

Comparison of Global rms Deviations. Figure 4 displays a superposition of the time-dependent rms deviation of each of the six trajectories of **Set_16** conducted here generated with a 12−16 Å *solute−solvent* and *solvent−solvent* cutoff and a superposition of the time-dependent rms deviation of each of the eight trajectories of **Set_8** generated in a preceding work with an 8 Å *solute−solvent* and *solvent−solvent* truncation distance.[29] Trajectories showing the lowest and highest rms deviation from the crystal structure at the end of the 100 ps of simulation time for each set are in bold and the time average trajectory of each set is plotted in dotted bold. The calculated rms spread at the end of the trajectory for **Set_16** was 1.6 Å and the trajectory averaged rms deviation was 1.3 Å. For **Set_8**, these values became 2.2 and 2.3 Å, respectively. Thus, in **Set_16** relative to **Set_8**, the rmsd range of the set was reduced and, as a whole, the rmsd values of the individual trajectories were seen to decrease.

Comparison of rms/Residue Profiles. Figure 5 shows the ensemble profiles obtained for the rms/residue averaged values for both sets. This average was taken over the last 5 ps of each trajectory in order not to overrepresent data resulting from near the start of the MD which is the crystallographic reference. Again the curves corresponding to the trajectories with the highest and lowest global rms values are represented in bold and the curve corresponding to the time-average trajectory in dotted bold. For **Set_16**, the overall spread is relatively small. Loop residue m^1G37, however, displays a complete range of mobilities in the individual trajectories compared to the moderate mobility of residue G34. This is reflected in the trajectory averaged profile for **Set_16**, where the mobility of m^1G37 is averaged out. For **Set_8**, the spread of rms values for the profile is considerably greater and a complete range of mobilities for residue G34 is observed, although the trajectory averaged profile again identifies this residue as the most dynamically active. Leveling out of the time-average trajectory in the per-residue rmsd profile is observed for **Set_16**. In both sets, the

(31) Auffinger, P.; Beveridge, D. L. *Chem. Phys. Lett.* **1995**, *234*, 413−415.
(32) Pearlman, D. A.; Case, D. A.; Caldwell, J. W.; Ross, W. S.; Cheatham, T. E., III; Ferguson, D. M.; Seibel, G. L.; Singh, U. C.; Weiner, P. K.; Kollman, P. A. *AMBER 4.1*; San Francisco, CA, 1994.
(33) Westhof, E.; Dumas, P.; Moras, D. *J. Mol. Biol.* **1985**, *184*, 119−145.
(34) Pearlman, D. A.; Kim, S. H. *J. Mol. Biol.* **1990**, *211*, 171−187.
(35) Singh, U. C.; Brown, F. K.; Bash, P. A.; Kollman, P. A. *J. Am. Chem. Soc.* **1987**, *109*, 1607−1614.
(36) van Gunsteren, W. F.; Berendsen, H. J. C. *Angew. Chem., Int. Ed. Engl.* **1990**, *29*, 992−1023.
(37) Avbelj, F.; Moult, J.; Kitson, D. H.; James, M. N. G.; Hagler, A. T. *Biochemistry* **1990**, *29*, 8658−8676.
(38) Ryckaert, J. P.; Ciccotti, G.; Berendsen, H. J. C. *J. Comput. Phys.* **1977**, *23*, 327−336.
(39) Engler, E.; Wipff, G. *MDdraw: A Program to Visualize MD Trajectories*; Université de Strasbourg, France, 1994.

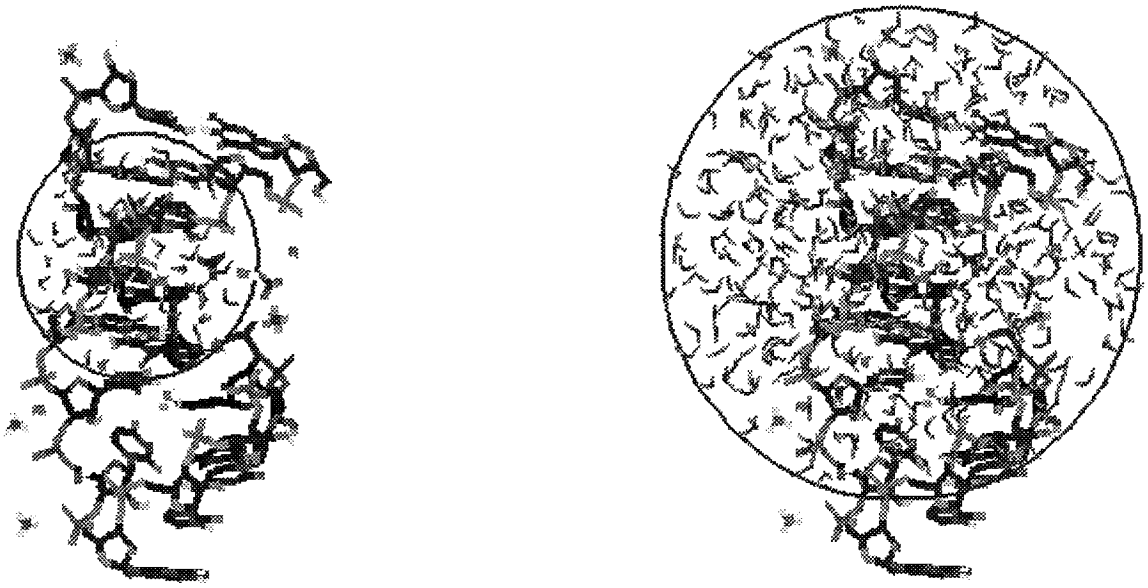

Figure 2. At left, the 8 Å solvation sphere around the phosphorus atom of residue G30; at right, the 16 Å solvation sphere around the same atom.

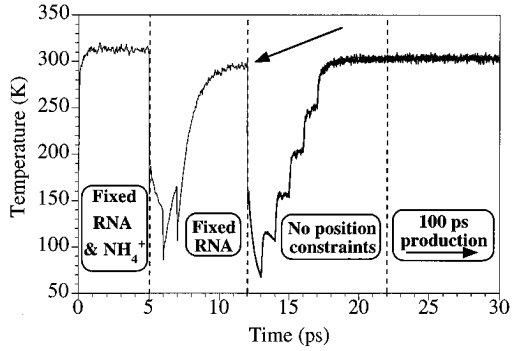

Figure 3. Superposition of the curves representing the evolution of the temperature with time during the equilibration procedure of the six trajectories of **Set_16**. The arrow, at $t = 12$ ps, indicates the change in velocity distribution at the 50 K restart for each of the six trajectories of this set.

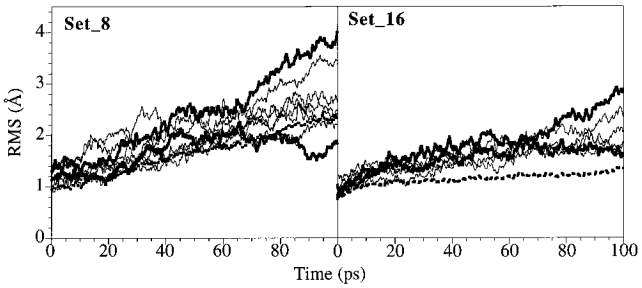

Figure 4. Superposition of the curves representing the total rms deviations with respect to the crystal structure for the 100 ps of production for **Set_8** (left) and **Set_16** (right). The trajectories with the respectively lowest and highest final rms deviations are plotted in bold, and the curves corresponding to the average trajectories are plotted in dotted bold.

high deviations of the first residues observed for some trajectories have been attributed to an unwinding of the stem which could result from the reduction of our system to a five base pair stem not connected to the rest of the tRNA structure.

Structural Transitions in the Sugar−Phosphate Backbone. Calculated dihedral transitions of the backbone are shown in Table 1. For **Set_16**, an average of 6.5 transitions per 100 ps is observed. This contrasts with the 15 transitions per 100 ps calculated for **Set_8**. Most of the observed backbone transitions occur during the 100 ps of production of each trajectory, while

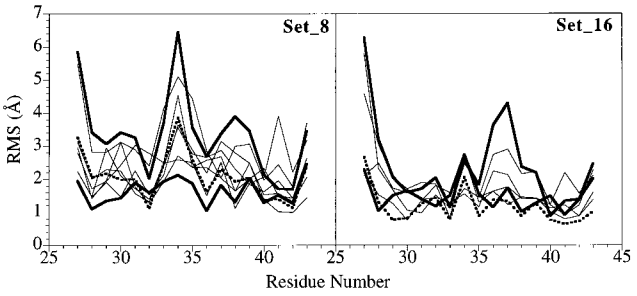

Figure 5. Superposition of the curves representing the rms deviations per residue averaged over the last 5 ps of each trajectory for **Set_8** (left) and **Set_16** (right). The trajectories with the respectively lowest and highest final rms deviations are plotted in bold, and the curves corresponding to the average trajectories are plotted in dotted bold.

Table 1. Average Number of Backbone Dihedral Transitions[a] per 100 ps of Simulation for **Set_8** and **Set_16**

	Set_8	**Set_16**
P−O5′−C5′−C4′	1.5	0.3
O5′−C5′−C4′−C3′	4.1	2.7
C5′−C4′−C3′−O3′	none	none
C4′−C3′−O3′−P	1.6	0.5
C3′−O3′−P−O5′	1.2	0.2
O3′−P−O5′−C5′	6.5	2.8
Total :	*15*	*6.5*

[a] Dihedral transitions are defined as transitions between minima centered respectively on the g^+ domain (+60°), the g^- domain (−60°), and the t domain (180°).

none of them are observed for **Set_16** during the equilibration phase, and only a small number for **Set_8**. No transitions are observed around the glycosyl dihedral angle linking the sugar to the bases or around the C4′−C3′ dihedral angle (i.e. sugar puckers) in both sets. Transitions around C5′−C4′ and P−O5′ dihedral angles are most frequently observed and found at various positions of the stem and the loop. Interestingly, this occurs with the same frequency in both sets. The only O5′−C5′ transitions observed take place between residues G34 and U35 in the loop of the anticodon and are much less frequent for **Set_16** than for **Set_8**. In fact, only one reversible transition is observed in one trajectory of this set. Transitions around the C3′−O3′ and O3′−P dihedral angles are only observed in the loop for both sets.

Table 2. Average Distances and Angles (in Italic) of Some Structurally Important Hydrogen Bonds of the Stem and Loop of the Anticodon Fragment Averaged Over 40 ps Made of the Last 5 ps of Each Trajectory in **Set_8** and Over 30 ps Made of the Last 5 ps of Each Trajectory in **Set_16**

	Set_8[a]		**Set_16**[a]		exp[b]
		Stem Hydrogen Bonds			
G27−C43[c]					
O6···H4−N4	1.94 (0.11)	<1.71−2.34>	1.93 (0.10)	<1.68−2.21>	1.92
	153 (14)	*<110−179>*	*151 (13)*	*<111−179>*	*161*
N1−H1···N3	1.90 (0.08)	<1.74−2.14>	1.92 (0.08)	<1.71−2.21>	1.82
	161 (10)	*<125−180>*	*155 (12)*	*<116−177>*	*175*
N2−H2···O2	1.89 (0.08)	<1.70−2.20>	1.91 (0.10)	<1.70−2.31>	1.90
	160 (10)	*<122−179>*	*159 (11)*	*<123−178>*	*168*
G28−C42					
O6···H4−N4	1.94 (0.16)	<1.71−2.97>	1.93 (0.18)	<1.66−3.21>	1.90
	156 (12)	*<103−179>*	*155 (14)*	*<107−178>*	*170*
N1−H1···N3	1.94 (0.10)	<1.70−2.43>	1.93 (0.10)	<1.74−2.52>	1.82
	159 (11)	*<119−180>*	*161 (10)*	*<127−179>*	*176*
N2−H2···O2	1.87 (0.10)	<1.67−2.21>	1.88 (0.11)	<1.65−2.49>	1.90
	159 (10)	*<131−179>*	*158 (12)*	*<118−178>*	*169*
C29−G41					
N4−H4···O6	2.26 (0.72)	<1.67−4.67>	2.28 (0.75)	<1.70−4.42>	1.93
	145 (16)	*<105−179>*	*147 (15)*	*<108−179>*	*158*
N3···H1−N1	2.26 (0.57)	<1.73−4.07>	2.12 (0.45)	<1.72−3.68>	1.83
	155 (14)	*<116−179>*	*159 (10)*	*<122−179>*	*172*
O2···H2−N2	2.36 (1.24)	<1.70−6.58>	1.99 (0.32)	<1.69−3.46>	1.89
	151 (14)	*<107−179>*	*156 (13)*	*<120−179>*	*175*
G30···U40					
O6···H3−N3	1.87 (0.14)	<1.65−2.90>	1.84 (0.08)	<1.62−2.27>	1.83
	156 (12)	*<114−179>*	*169 (9)*	*<124−179>*	*168*
N1−H1···O2	1.97 (0.20)	<1.65−3.02>	1.90 (0.13)	<1.68−2.57>	1.84
	147 (16)	*<93−178>*	*156 (12)*	*<117−179>*	*163*
C31−G39					
N4−H4···O6	2.19 (0.53)	<1.69−4.18>	1.92 (0.14)	<1.71−3.03>	1.94
	144 (22)	*<71−*179>	*156 (12)*	*<118−177>*	*157*
N3···H1−N1	2.04 (0.22)	<1.70−3.19>	1.93 (0.08)	<1.74−2.23>	1.83
	153 (12)	*<121−179>*	*161 (9)*	*<137−178>*	*169*
O2···H2−N2	1.93 (0.16)	<1.68−2.79>	1.88 (0.10)	<1.70−2.32>	1.88
	152 (14)	*<106−179>*	*162 (9)*	*<131−178>*	*177*
		Loop Hydrogen Bonds			
Ψ32···C38					
O4···H41−N4	3.53 (1.94)	<1.75−7.59>	2.59 (0.32)	<1.87−4.01>	2.89
	138 (25)	*<64−178>*	*95 (15)*	*<52−145>*	*105*
O4···H42−N4	4.64 (1.86)	<2.30−8.44>	2.59 (0.47)	<1.82−4.22>	2.68
	62 (17)	*<23−106>*	*96 (21)*	*<43−145>*	*92*
U33					
N3−H3···OA−P (C36)	2.34 (1.02)	<1.53−5.34>	1.75 (0.11)	<1.56−2.34>	2.13
	154 (13)	*<173−179>*	*161 (9)*	*<111−179>*	*134*
		Stacking between the U35 Phosphate and the U33 Base[d]			
	5.62 (1.14)	<3.92−8.55>	4.27 (0.33)	<3.64−5.50>	4.12

[a] Average values are in Å for the distances and in deg for the angles; rms fluctuations are given in parentheses; minimum and maximum values for each set are given in angle brackets. [b] Estimated on the basis of crystallographic coordinates of heavy atoms (in Å or in deg).[33] [c] The hydrogen bonds at first base pair, G27−C43, of the stem are constrained. [d] Distance between the 5′-phosphorus atom of U35 and the geometrical center of the six heavy atoms of the U33 ring.

Intramolecular Hydrogen Bonds. In our simulations, all the canonical hydrogen bonds between base pairs in the stem are on the average maintained at the end of 100 ps of simulation for both sets and for the regular Watson−Crick base pairs as well as for the noncanonical G30···U40 base pair with average distances close to 2.0 Å and average angle values around 155° (Table 2). However, partial fraying of some base pairs is observed as indicated by certain high upper hydrogen bond distance values (>3.0 Å) especially for the base pairs flanking the G30···U40 base pair, C29−G41 and C31−G39.

Other types of hydrogen bonds found in loops of ribonucleic acids appear equally essential for maintaining the three-dimensional structure of these fragments. In the anticodon loop of $tRNA^{Asp}$, the hydrogen bond (Ψ32)O4···H4−N4(C38) builds a "pseudo" base pair sandwiched between the end of the stem and the loop itself. For **Set_16**, we note that this hydrogen bond is relatively stable with an average distance of 2.6 Å and a maximum value of 4.2 Å. The average value of the angle has been calculated to be around 95°, close to the estimated crystallographic value. In **Set_8**, the (Ψ32)O4···H4−N4(C38) bond has a higher average value of 3.5 Å and fluctuates between 1.8 and 8.4 Å over the last 5 ps of each trajectory.

Another important hydrogen bond, (U33)N3−H3···OA−P(C36), stabilizes the U-turn of the loop.[33,40] For **Set_16**, this bond remains nicely preserved at the end of each simulation, with minimum and maximum distances between 1.6 and 2.3 Å and an average of 1.8 Å. The average distance calculated for the simulations of **Set_8** was 2.3 Å with values between 1.5 and 5.3 Å and associated 1.0 Å fluctuations. This indicates that the bond is on average not as well maintained during the 100 ps of MD as for **Set_16**. A further consequence of the lability of this bond for **Set_8** is that the stacking between the U33 base and the phosphate at the 5′ end of U35 fluctuates between 3.9 and 8.6 Å over the last 5 ps of each trajectory.

(40) Westhof, E.; Sundaralingam, M. *Biochemistry* **1986**, *25*, 4868−4878.

Table 3. Average Distances and Angles (in Italic) of Some Structurally Important C−H···O Hydrogen Bonds of the Stem and Loop of the Anticodon Fragment Averaged Over 40 ps Made of the Last 5 ps of Each Trajectory in **Set_8** and Over 30 ps Made of the Last 5 ps of Each Trajectory in **Set_16**

	Set_8[a]		**Set_16**[a]		exp[b]
Stem and Loop Intraresidue Hydrogen Bonds					
C8−H8···O5′					
G28	2.53 (0.24)	<2.10−3.51>	2.87 (0.58)	<2.20−4.33>	2.72
	136 (12)	*<104−168>*	*129 (11)*	*<103−160>*	*138*
G30	3.02 (0.53)	<2.18−4.50>	3.57 (0.91)	<2.17−5.29>	3.81
	130 (15)	*<78−167>*	*130 (9)*	*<106−157>*	*136*
G34	2.84 (0.39)	<2.05−4.41>	2.56 (0.18)	<2.20−3.18>	3.11
	111 (21)	*<59−158>*	*128 (20)*	*<80−169>*	*111*
m^1G37	3.00 (0.55)	<2.20−4.55>	2.68 (0.39)	<2.13−3.83>	3.01
	133 (15)	*<85−167>*	*135 (12)*	*<101−163>*	*126*
G39	2.50 (0.18)	<2.16−3.21>	2.49 (0.18)	<2.12−3.18>	2.65
	142 (10)	*<112−167>*	*129 (11)*	*<99−162>*	*164*
G41	2.45 (0.18)	<2.12−3.06>	2.64 (0.33)	<2.16−2.96>	2.71
	129 (16)	*<90−169>*	*134 (17)*	*<89−168>*	*142*
C6−H6···O5′					
C29	2.68 (0.32)	<2.11−3.86>	2.97 (0.73)	<2.12−4.79>	2.66
	140 (14)	*<101−173>*	*143 (15)*	*<103−178>*	*145*
C31	3.41 (0.74)	<2.26−5.12>	2.47 (0.15)	<2.12−3.08>	3.12
	139 (16)	*<99−175>*	*146 (12)*	*<102−177>*	*131*
Ψ32	3.03 (0.42)	<2.20−4.40>	2.39 (0.14)	<2.10−2.98>	2.57
	152 (9)	*<122−175>*	*135 (20)*	*<89−178>*	*161*
U33	3.90 (0.49)	<2.56−5.00>	2.67 (0.22)	<2.15−3.31>	2.70
	137 (9)	*<116−164>*	*154 (9)*	*<122−176>*	*148*
U35	3.61 (0.56)	<2.27−4.92>	2.87 (0.53)	<2.20−4.40>	2.61
	136 (12)	*<89−167>*	*152 (10)*	*<122−177>*	*150*
C36	3.29 (0.63)	<2.21−4.72>	3.00 (0.74)	<2.11−4.63>	2.08
	146 (9)	*<119−168>*	*145 (17)*	*<91−176>*	*166*
C38	3.51 (0.67)	<2.32−4.96>	2.40 (0.16)	<2.05−3.38>	2.24
	141 (13)	*<110−173>*	*136 (12)*	*<100−175>*	*161*
U40	2.93 (0.63)	<2.13−4.67>	2.76 (0.35)	<2.10−3.71>	2.61
	144 (12)	*<105−173>*	*145 (9)*	*<120−172>*	*141*
C42	2.71 (0.30)	<2.16−3.75>	2.55 (0.21)	<2.15−3.18>	2.20
	150 (10)	*<121−176>*	*145 (11)*	*<111−177>*	*156*
C43[c]	3.59 (0.46)	<2.48−4.66>	3.08 (0.51)	<2.26−4.54>	2.05
	142 (9)	*<116−171>*	*143 (10)*	*<107−171>*	*169*
Loop Interresidue Hydrogen Bonds					
U33···C36					
O2···H5-C5	3.43 (0.96)	<2.21−6.43>	2.71 (0.42)	<2.13−3.88>	2.07
	140 (20)	*<95−179>*	*133 (20)*	*<95−178>*	*166*
U33···U35					
O2′···H5-C5	3.62 (1.44)	<2.22−8.16>	2.60 (0.30)	<2.13−3.79>	2.28
	121 (18)	*<74−168>*	*130 (25)*	*<80−176>*	*136*

[a] Average values for the H···O distances and C−H···O angles are in Å and deg respectively; rms fluctuations are given in parentheses; minimum and maximum values for each set are given in angle brackets. [b] Estimated on the basis of crystallographic coordinates of heavy atoms (in Å or in deg).[33]

C−H···O Hydrogen Bonds. C−H···O hydrogen bonds between C−H groups and acceptor atoms can be identified in the crystal structure of $tRNA^{Asp}$ and may help to maintain the three-dimensional shape of the anticodon loop. The intraresidue (C8)H8···O5′ hydrogen bond in guanosine residues is present in all guanines, in both the stem and the loop, in both sets of MD trajectories with individual trajectory hydrogen bond distance averages of 3.0 Å or less (Table 3) and minimum values around 2.2 Å (with the exception of the average value of 3.6 Å calculated for residue G30 in **Set_16** in accord with the estimated crystallographic value of 3.8 Å). The average angular values are located around 130° with maxima of 180° indicating the occurrence of linear interactions. The possible (C6)H6···O5′ intraresidue hydrogen bonds seem to be equally satisfied for pyrimidines in **Set_16** with minimum values sometimes under 2.2 Å, but are found to be not as stable for the **Set_8** trajectories where calculated average values for all the loop residues are over 3.0 Å. The average angular values for the (C6)H6···O5′ bonds are slightly higher than for the (C8)H8···O5′ bonds, 145° instead of 130°.

Two non-standard C−H···O hydrogen bonds are also found in the loop. The (U33)O2···H5−C5(C36) bond (estimated X-ray value 2.1 Å; Figure 6), with an average value of 2.7 Å calculated in **Set_16**, is conserved in four simulations of the set. In the two other trajectories, the (U33)O2 oxygen atom preferentially makes a hydrogen bond with the (C36)N4−H41 hydrogen atom. For **Set_8**, and as seen for the other hydrogen bonds of the loop, this bond displays reduced stability with a calculated averaged value of 3.4 Å over the five last picoseconds of the trajectories and a maximum value of 6.4 Å. A similar situation is found for the (U35)C5−H5···O2′(U33) hydrogen bond (estimated X-ray value 2.3 Å; Figure 7), which is conserved for four of the six 100-ps trajectories of **Set_16**. For the two other simulations, this bond is maintained for approximately 20 ps and then is relinquished in favor of two other independent interactions, one between the (C36)N4−H41 of the upper base and the (U33)O2′ hydroxyl oxygen atom while the other (U35)C5−H5 hydrogen atom establishes a second "stable" C−H···O interaction with (U33)O3′. Maxima close to 180° for the calculated angular values are indicative of the occurrence of linear interactions for these bonds.

Comparison of the Lowest rms Trajectories from Both Sets. Looking back at Figure 4, one may note that some trajectories in both sets show similar low rms deviations from

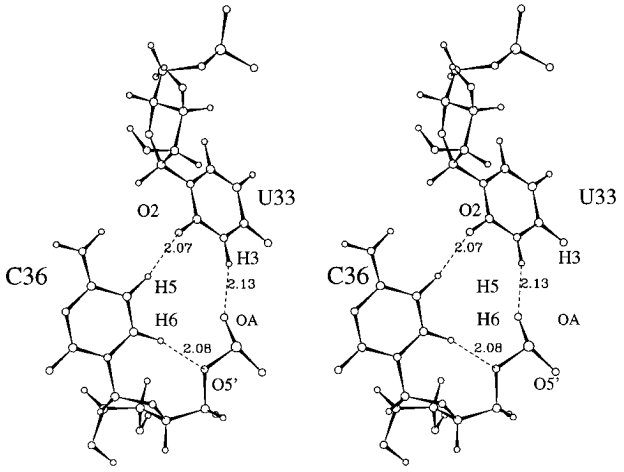

Figure 6. Stereoview of the two C−H···O and one N−H···OA hydrogen bonds observed between U33 and C36 in the crystallographic structure (hydrogen atom positions have been estimated).

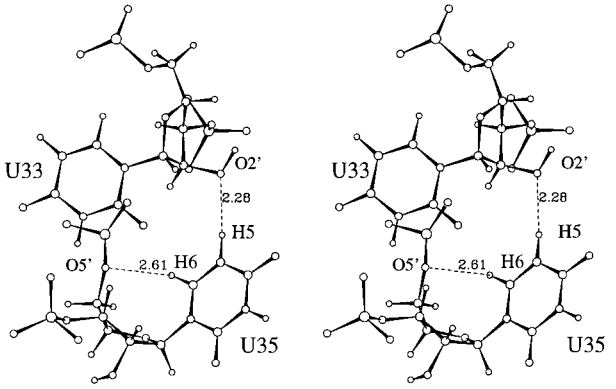

Figure 7. Stereoview of the two C−H···O hydrogen bonds observed between U33 and U35 in the crystallographic structure (hydrogen atom positions have been estimated).

the crystal structure and could be considered comparable with respect to the rms deviation criteria. To explore this possibility, the lowest rms trajectories of each set are compared in more detail to discern the character of the two MD protocols. In Figure 8, a comparison is shown of the time course of the distances between hydrogen-bonded pairs in the seven-base anticodon loop for the two simulations having the lowest rms values (called **Low_rms_16** and **Low_rms_8**). These bonds are (Ψ32)O4···H41−N4(C36), (U33)N3−H3···OA−P(C36), (U33)O2···H5−C5(C36), and (U35)C5−H5···O2′(U33). In addition, the distances calculated for the stacking between the base ring of residue U33 and the phosphate group of U35 which stabilizes the U-turn are also shown. The reduced dynamical variation for **Low_rms_16** relative to **Low_rms_8** is apparent even though the final rms deviations averaged over the last 5 ps of the two trajectories are quite similar: 1.6 Å for **Low_rms_16** and 1.8 Å for **Low_rms_8**. Thus, although stabilized rms deviations do indicate that the system has settled in a local minima of the conformational space, the rms deviation criteria has to be considered in the context of specific local structural and dynamical data in order to assess the dynamical character and relative structural stability of an individual MD trajectory.

Discussion

In our effort to produce useful MD simulations of the anticodon loop of $tRNA^{Asp}$, we have refined the protocol used in our first study by increasing the long-range truncation distance for *solvent* interactions from 8 to 16 Å using a 12−16 Å twin-

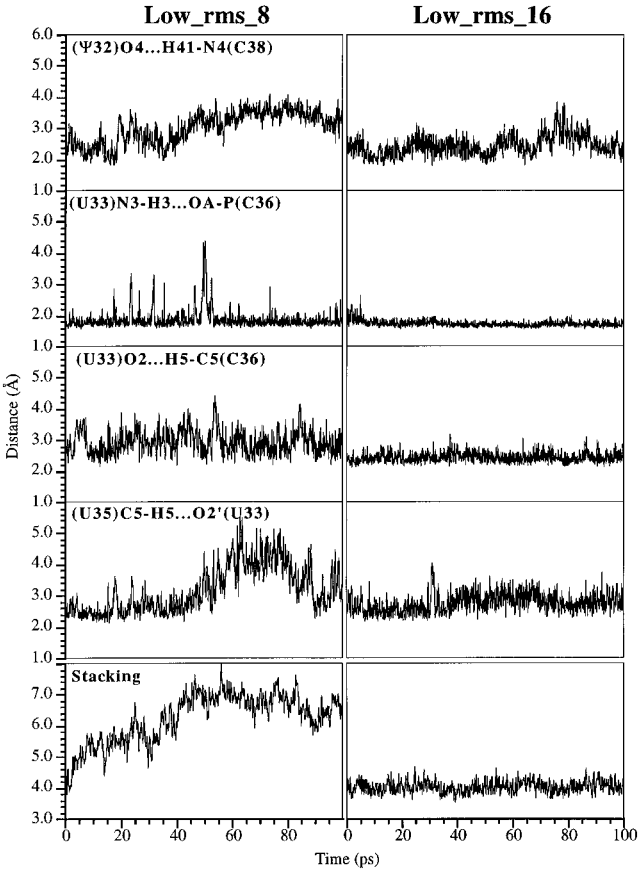

Figure 8. Time evolution of some selected hydrogen bonds and of the stacking distance between the geometrical center of the U33 ring and the U35 phosphorus atom for the two simulations of both sets having the lowest rms deviation values, **Low_rms_8** (final rmsd 1.8 Å) and **Low_rms_16** (final rmsd 1.6 Å), represented in bold in Figures 4 and 5.

range cutoff, while calculating explicitely all *solute−solute* interactions. In order to assess the consistency of the present protocol and the extent of structural stability of the solute conformations generated in the MD trajectories, we have employed strategy using multiple molecular dynamics simulations.[29] Specifically, this strategy consists of generating several short trajectories starting from the same initial configuration but with different initial velocitiy distributions. Given the available computational resources, we restricted ourself to the generation of six 100-ps independent trajectories. We do not claim to have demonstrated an equilibrated system on the 100 ps time scale. However, from the structural and dynamic diversity of the generated trajectories and from the comparison of the two sets presented here, it has been possible to extract, on a broader statistical basis, useful theoretical and structural information concerning both MD methodology and the possible tertiary structural stabilizations of the $tRNA^{Asp}$ anticodon hairpin fragment in the region of the starting configuration. Specifically, we address the question of the effect of long-ranged hydration forces on the system stability and on the solute conformation and dynamics. Further, the MD trajectories were used to assess the possible contribution of C−H···O hydrogen bonds potentially present in the crystal structure to the stabilization and the maintenance of the tertiary structure of the tRNA fragment.

System Stabilization. From **Set_16** to **Set_8** the rms spread for the ensemble of trajectories was reduced from 2.2 to 1.6 Å and the trajectory averaged rms deviation of both sets dropped from 2.3 to 1.3 Å (Figure 4). Figure 5 shows two very different ensemble profiles obtained for the rms/residue values averaged over the last 5 ps of each trajectory for both sets, again showing

smaller values and lower spread for **Set_16** relative to **Set_8**. Thus, a considerable degree of system stabilization seems to have been effected by the inclusion of long-ranged hydration forces. This is further supported by a closer look at the dynamics of specific tertiary interactions of the loop region as shown in Figure 8, for the lowest rms trajectory of each set. In several instances, either the amplitude of dynamics, the range of time-dependent values, or both are minimized in **Set_16** relative to **Set_8**, a likely contribution to the improved structural stabilization of the U-turn found in **Set_16**.

It is interesting to note that for **Set_16**, the calculated final 1.3 Å rms deviation for the averaged trajectory is lower than the rms deviations calculated for any of the individual trajectories. A similar situation has also been observed for simulations of proteins in their crystallographic environment where the unit cell average structures are closer to the crystallographic structure at the end of the simulation time than the individual monomers.[9−11,37] In Figure 5 leveling out of the trajectory averaged per-residue rmsd profile, observed for **Set_16**, suggests that in general the residues occupy localized regions of the configurational space where again the average calculated position for these residues is closer to the crystallographic structure than any of the values calculated from individual trajectories. This may reflect a computational analogy to the time and ensemble averaging inherent to both crystallographic[41] and NMR methods[42] and is a further advantage of the multiple trajectory molecular dynamics approach.

Tertiary Structure Stabilization. The occurrence of dihedral angle transitions listed in Table 1 for the two sets of MD trajectories reveals less than half as many transitions when long-range hydration forces are included in the MD electrostatic model. Because a substantial number of transitions are observed in the loop region, where their effect on the tertiary interactions preserving the native conformation of the loop can have a substantial effect, the reduction of the number of transitions in **Set_16** relative to **Set_8** is significant.

A tertiary interaction not well conserved in the **Set_8** trajectories is the hydrogen bond (Ψ32)O4···H41−N4(C38). Experimentally the stability of this interaction has been questioned[33] since large temperature factors in this region and the absence of explicit hydrogen atoms in the electron density maps of the macromolecular crystallography make it difficult to discern the nature of this interaction. Although the upper bound of this bond in **Set_16** (4.0 Å) reveals it to be more labile than a canonical base pair hydrogen bond, it is found to be relatively stable with an average distance of 2.6 Å. The (U33)N3−H3···OA−P(C36) hydrogen bond remains nicely preserved at the end of all the individual trajectories for **Set_16** with an average of 1.8 Å over the ensemble of trajectories. For the **Set_8** ensemble, however, these interactions show potentially disrupting dynamics character as demonstrated in Figure 8.

Since both MD sets were started from the exact same initial solute configuration with explicit calculation of all *solute−solute* interactions, the observed improvement of the structural and dynamical characteristics of the solute can only be attributed to the inclusion of long-range *solute−solvent* and *solvent−solvent* interactions. In summary, the inclusion of long-range *solvent* interactions in the present MD protocol led to dramatic improvement of the structural and dynamical characteristics of the solute itself. The overall rms deviations were lower for **Set_16**, as shown in Figure 4, and contrary to the simulations of **Set_8**, key structural hydrogen bonds of the loop were better preserved in **Set_16** trajectories. It can be reasoned that the increase of the truncation distances for **Set_16** leads to a solvent reorganization around the RNA fragment which changed the relative energetic balance for the interactions involving the solvent.[43] Thus, it appears that the structural stability of the anticodon loop is related not only to a correct description of the main *solute−solute* interactions or to water in the first hydration shell of the solute but also to a great extent to long-ranged *solute−water* and *water−water* interactions, which could as well play a determining role in RNA folding processes.

Structural Role of C−H···O Hydrogen Bonds. In the present work, most of the potential purine C8−H8···O5′ and pyrimidine C6−H6···O5′ hydrogen bonds satisfying standard hydrogen bonding distances and angles are present to some extent in both sets of trajectories (Table 3). The two unusual (U33)O2···H5−C5(C36) and (U35)C5−H5···O2′(U33) hydrogen bonds observed in the anticodon loop are found to be stable over 100 ps for four of the six trajectories of **Set_16**. For the two remaining simulations they broke after approximately 20 ps and were replaced, in one case, by an alternate stable C−H···O3′ hydrogen bond. Thus, the extent of satisfied potential C−H···O hydrogen bonds, both in the stem and the loop, strongly suggests that such C−H···O bonds participate in the stabilization of the tertiary structure of this RNA loop possibly by adding a small enthalpically favorable contribution to the total hydrogen bond energy. Because the free energy balance in biomolecular systems is very subtle, these C−H···O interactions could, in some cases, be structure determining or play a role in complexation processes.

Such bonds are most likely present in other RNA or DNA structures as there is a high occurrence of C−H groups of acidic character in nucleic acid bases. Their possible structural contributions emphasize the need for the use of all atom force fields in molecular dynamics simulations of biomolecules. Furthermore, given their electrostatic nature, the partial charges on the hydrogen atoms attached to a carbon need to be parametrized as accurately as polar substituents have been. Comparison with simulations of other tRNA sequences of the anticodon loop would help further characterize their structural importance.

Future Considerations. Even with augmented truncation distances, the rms values of some trajectories in **Set_16** are still increasing at the end of the 100 ps of simulation time. The size of the truncation distance that needs to be used in molecular dynamics simulations in order to minimize possible artifacts is probably much longer than is practical for current computer resources. As truncation distances are increased, it is possible that the artifacts still present will manifest their effects on longer time scales, as the feedback of artificial correlations occurring at the cutoff sphere to the short-range order would have longer, probably system-dependent, relaxation times. Ewald summation methods are an alternative to the use of truncation distances and have, among others, the advantage of accurately calculating long-range interactions while producing smooth forces at all distances. Preliminary results of the same $tRNA^{Asp}$ anticodon loop system subjected to an MD protocol utilizing the Particle Mesh Ewald (PME) technique[10,44] for calculating the electrostatic interactions display a decrease in the average rms deviations to 0.9 Å on the 100 ps time scale as compared to the 1.3 Å average rms deviations calculated here for the 16 Å

(41) Edholm, O.; Berger, O.; Jähnig, F. *J. Mol. Biol.* **1995**, *250*, 94−111.
(42) Bonvin, A. M. J. J.; Brünger, A. T. *J. Mol. Biol.* **1995**, *250*, 80−93.
(43) Chervenak, M. C.; Toone, E. J. *J. Am. Chem. Soc.* **1994**, *116*, 10533−10539.
(44) Darden, T.; York, D.; Pedersen, L. *J. Chem. Phys.* **1993**, *98*, 10089−10092.

truncation distance.[45] However, the Ewald methods are certainly not artifact free and may introduce long-range correlation in the system. Detailed structural analyses are underway to reveal the differences in the solute structure and dynamics for these two methods.

Conclusions

We have made a comparison of two sets of trajectories in which the long-ranged *solvent* interactions have been more accurately accounted for by extending the truncation distances for interactions involving the solvent. Modifying only the truncation distances for the interactions with the solvent between the two sets allowed for a clear demonstration of the effects associated with the inclusion of long-range *solvent* interactions, generally neglected in MD calculations. The results described here emphasize that complete treatment of all interactions, even the most subtle ones like long-ranged solvation forces or weak C−H···O hydrogen bonds, are likely necessary to maintain the structural integrity of such complex biomolecules. Furthermore, the multiple molecular dynamics strategy has been shown to be a very useful tool in the validation process of simulation protocols, as it allowed for a more efficient sampling of the theoretical configurational space around the starting configuration and a comparison on a broader basis of the two sets of trajectories discussed here.

Acknowledgment. P.A. is supported by a fellowship from ORGANIBIO (28, rue Saint Dominique, Paris, France) in the program CM_2AO. S.L.-M. is grateful to the French government for providing a Chateaubriand fellowship. The authors also acknowledge the IDRIS computing center which provided computer time and E.W. is thankful to the CEE for providing funds through the Biotech contract BIO 2-CT93-0345.

JA952494J

(45) Louise-May, S.; Auffinger, P.; Westhof, E. Biological Structure and Dynamics. In *Proceedings of the Ninth Conversation, State University of New York*; Sarma, R. H., Sarma, M. H., Eds.; Adenine Press: Albany, NY, in press.